RESEARCH ARTICLE

Ensemble streamflow projections for a small watershed with HSPF model

Mine Albek[1] · Erdem Ahmet Albek[1] · Serdar Göncü[1] · Burcu Şimşek Uygun[1]

Abstract

A watershed modeling tool, Hydrological Simulation Program-FORTRAN (HSPF), was utilized to model the hydrological processes in the agricultural Sarısu watershed in western Turkey. The meteorological input data were statistically downscaled time series from General Circulation Model simulations. The input data were constructed as an ensemble of 400 individual time series of temperature, precipitation, dewpoint temperature, solar radiation, potential evapotranspiration, cloudiness, and wind velocity, as required by HSPF. The ensemble was divided into four subsets, each comprising of 100 time series, of different Special Report on Emissions Scenarios. Yearly and monthly total streamflow time series were obtained from the calibrated and validated HSPF model spanning a period of 116 years between the water years of 1984 and 2099. The projections in the watershed showed a median increase of 3 °C in yearly average temperatures between the beginning and end 30-year periods of the 116-year simulation periods based on 400 ensemble members while the corresponding change in total yearly precipitation was − 71 mm. These changes led to a decrease in yearly streamflows by 40% which reflected itself to varying degrees in monthly flows. Correlations were established between the principal drivers of the watershed hydrological cycle, namely temperature and precipitation, and streamflow. The results showed that the changes in the climatic conditions will greatly affect water-related issues in the watershed and emphasize the necessity of preparing carefully to adapt to a warmer and drier climate.

Keywords Climate change · Statistical downscaling · Watershed · HSPF · Streamflow · Hydrological modeling · Correlation · Nonparametric analysis

Introduction

It is well known that earth's climate is undergoing a change unparalleled in recent human history since the industrial revolution which carries with it serious risks for the earth. Climate change primarily shows itself in changing temperatures, mostly on the increasing size, alterations in precipitation quantities and patterns, and rising sea levels. Simulations with general circulation models (GCMs) based on emission scenarios indicate also that the climate will continue to change in the twenty-first century. Temperatures are projected to increase almost all over the earth, while precipitation varies among regions in trend direction (IPCC 2007; NRC 2010). Thus, changes are present and are projected to continue in the two principal drivers of the hydrological cycle and these threaten sufficient and good quality water supply to meet the increasing domestic, industrial, and agricultural demands. Careful and adequate management of water as a renewable but limited natural resource is imperative in this respect.

In making projections into the future, both for estimating the quantitative extent of climate change and determining again the quantitative effects of this change on watershed processes and the resulting watershed output, the use of models is indispensable. Models, though they are based on certain assumptions, can create a near-realistic abstraction of the future

✉ Burcu Şimşek Uygun
bsimsek1@eskisehir.edu.tr

Mine Albek
mlule@eskisehir.edu.tr

Erdem Ahmet Albek
ealbek@eskisehir.edu.tr

Serdar Göncü
sgoncu@eskisehir.edu.tr

1 Faculty of Engineering, Environmental Engineering Department, Eskişehir Technical University, Iki Eylül Campus, Eskişehir, Turkey

and be very useful in making plans to manage the future, as long as the assumptions are known and their impact on the results anticipated.

Many models were used for simulating watershed behavior under climate change scenarios. A widely used and comprehensive mechanistic watershed model is HSPF (Hydrological Simulation Program-FORTRAN). There are a number of studies done with HSPF concerning the effects of climate change on watershed processes and subsequent watershed outputs (Abdulla et al. 2009; Al-Abed and Al-Sharif 2008; Baloch et al. 2015; He et al. 2013; Yan et al. 2014). Ng and Marsalek (1992) studied a small 53-km^2 watershed in Canada with respect to the effects of changes in climate inputs on the streamflow emanating from the watershed. HSPF was calibrated first and, based on scenario predictions of a 4 °C increase in temperatures and a 10% increase or decrease in precipitation, these changes were integrated into the model. It was found out that a temperature increase of the magnitude mentioned above would decrease streamflows by 1%. Changes in precipitation together with the temperature increase changed streamflows considerably and resulted in increases in peak flows in winter months.

Albek and Albek (2003) modeled an agricultural watershed (Seydi Suyu) in Turkey and studied the climate change effects on the watershed output using HSPF. Different scenarios were created in which temperature and precipitation changed in different combinations and their effects investigated. In a companion study, it was found that a 3 °C increase in temperatures would lower streamflows by as much as 20% (Albek et al. 2004). Also, it was simulated with HSPF that coverage of the watershed with deep-rooted vegetation would increase the reductions in streamflow to 37%.

Goncu and Albek (2007) prepared climate change scenarios based on long-term climatic trends expected to occur in western Turkey and a hypothetical watershed was simulated with HSPF using different land uses. Both yearly and intermonthly variations in total outflow emanating from the watershed covered by pasture, deciduous forest, and barren land were investigated.

Climate change effects on streamflows leaving watersheds and on reservoir volumes were studied by Goncu and Albek (2010). HSPF was used to simulate the behavior of coniferous and deciduous forests, barren lands and pastures, and flood frequency analysis conducted. Significant differences were observed in streamflows and reservoir volumes between scenarios, soil types, and land uses. It was also observed that temperature and precipitation often acted to counterbalance their effects on longer time periods, but that they could reinforce their effects on a monthly basis. Lopez et al. (2013) used HSPF to simulate archetypal watersheds with urban, vegetated, and mixed urban/vegetated land covers to develop a framework for evaluating regional hydrologic sensitivity to climate change.

Studies are also present, conducted with HSPF, to find out how indices about the water quantity present in watersheds and how these indices change in response to climate change (Jun et al. 2011; Kim and Chung 2014). It was indicated in a number of studies, based on the result of before mentioned works, that design criteria to be considered for urban water construction works like stormwater networks would differ in future from the ones present (Mukundan et al. 2013; Rosenberg et al. 2010). There are studies which also incorporate city growth in the future and land use change, besides climate change scenarios to be able to predict future trends (Choi and Deal 2008; Chung et al. 2011; He and Hogue 2012; Mitsova 2014; Yang et al. 2012). Models like HSPF are used to aid in developing water management plans to abate the impacts of climate change (Ranatunga et al. 2014).

Besides works investigating the effects of climate change on the water quantity in watersheds, studies were also conducted to determine the effects on the water quality. Goncu and Albek (2008) used HSPF to study the impact of climate change on a dissolved water quality constituent (chloride) and suspended matter. Increased concentrations in watershed outflow chloride concentrations and sediment transport amounts were simulated with the SRES A2 scenario. Taner et al. (2011) used integrated models which also included HSPF to investigate impacts of climate change on a North American lake and found out a water temperature increase by as much as 5 °C during the 2040–2069 time periods.

The purpose of this study is the application of a model to a small stream system in order to predict the effects of climate change which manifests itself with increasing temperatures and mostly decreasing precipitations. HSPF is coupled with a climate model to investigate how watershed output (streamflow) evolves in response to the climate change projected in the climate model. This model is driven by meteorological input from general circulation models (GCM). GCM results were obtained from the respective centers (Canadian Centre for Climate Modelling and Analysis and Met Office Hadley Centre) which developed these models and distribute the simulation results (Canadian Centre for Climate Modelling and Analysis 2012; ECMWF ERA-40 data 2012; Kalnay et al. 1996; Kistler et al. 2001; Climate Impacts LINK Project 2012). These inputs with a coarse resolution were statistically downscaled to a particular watershed of interest (Göncü and Albek 2015). The downscaling enables the creation of ensembles of meteorological time series which can be fed into the respective watershed model to likewise obtain streamflow projection ensembles. Thus, the streamflow output is not presented as a single quantity measure, but with statistical indices based on the projection cloud. This type of analysis presents an uncertainty range which enables users of the projections not to limit their decisions and plans to a single output but to a range of likely outputs and consequently develop a more realistic approach and also to propose alternatives.

Study area

The Sarısu stream is a tributary of the Porsuk stream located within the Sakarya river watershed in the western portion of Inner Anatolia, Turkey (Fig. 1). The Sarisu watershed has a total surface area of 444 km^2 with elevations ranging between 865 and 1090 m above mean sea level. The stream is 54.3 km long and originates at the Dodurga reservoir, a small reservoir intended to supply irrigation water to the Sarısu watershed. The stream is surrounded by flat plains and moderately high hills border the floodplain. Forty-five percent of the area is covered by farmlands practicing non-irrigated agriculture. Pastures on the bordering hills constitute around 44% of the total area. Irrigated farmlands make up around 5% of the area. The rest is covered by barren lands and sparse forests (Fig. 1).

Yearly streamflow values aggregated from daily measurements are presented in Fig. 1. The year is not the calendar year but the water year which begins at October 1 and ends at September 30 the following year. This convention is applied in order not to split the winter season in which the majority of the precipitation falls between years. The measurements belong to the Sarısu-İnönü hydrological station operated by the General Directorate of State Hydraulic Works which is located 34 km behind the confluence of the Sarisu with the Porsuk stream (Monitoring Stations Management System 2010). Based on 13 yearly means beginning in the water year 1984 and ending in the 2004 water years with 8 missing years, the average yearly streamflow amounts to 16.7 Mm^3.

The watershed is dominated by a continental climate with maritime influences (Albek 2003). There are two meteorological stations on the outskirts of the watershed boundaries (Fig. 1) which possess long time high-frequency records. The Eskişehir station (17123) and the Bozüyük station (17702) are operated by the Turkish State Meteorological Service (TUMAS Meteorological Data Archive and Management System 2010). Based on records from the stations in the same period as the hydrological measurements but without any missing years, the average temperatures are 10.6 °C and 10.5 °C for 17123 and 17702, respectively. The precipitation amounts, however, differ considerably. In the 20 years from October 1, 1984 to September 30, 2004, the average recorded precipitation in the Eskişehir station is 348 mm while it is 495 mm for the Bozüyük station. Thus, the western part of the watershed receives around 42% more precipitation than the eastern part.

Modeling with HSPF

Model setup and meteorological input

For the modeling of the Sarısu watershed, the HSPF (Hydrological Simulation Program-FORTRAN) model which is a comprehensive simulation tool of the hydrological cycle and water quality at watershed scale is utilized. HSPF is a modular lumped parameter model with 3 modules for the
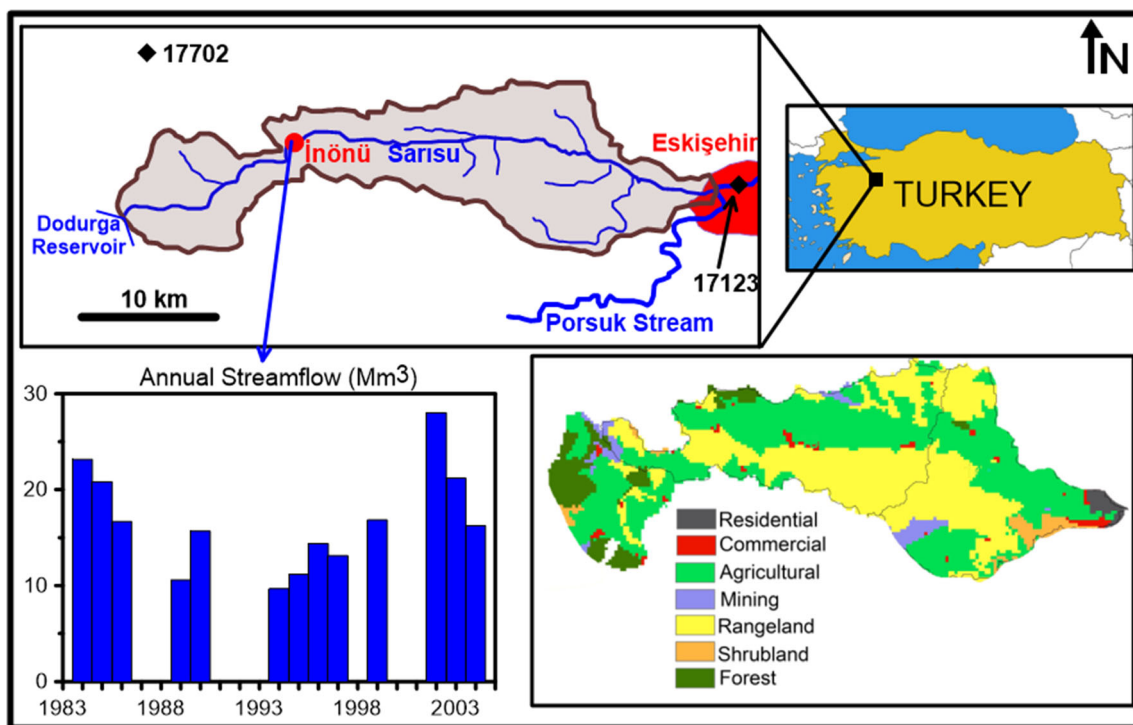

Fig. 1 The Sarısu watershed (upper left: watershed map; upper right: location of watershed in Turkey; lower left: yearly streamflow at the Sarısu-İnönü station; lower right: watershed land use)

simulation of processes in pervious land segments (PERLND), impervious land segments (IMPLND), and a free flowing water bodies (RCHRES) (Bicknell et al. 2001; Lumb et al. 1994).

The watershed was subdivided into nine pervious land segments based on the land use (farmland, pasture, irrigated field, forest, barren land, urban). Use of the BASINS interface to HSPF was utilized in the segmentation of the watershed (USEPA 2015) based on the land use maps. The stream was divided into two segments based on the change of the talveg slope. The land segments contribute flow to both stream segments in different amounts. The land and stream segments are described in Table 1.

HSPF makes use of seven required meteorological time series to derive the hydrological processes. These time series are temperature, precipitation, cloudiness, solar radiation, wind velocity, dewpoint temperature, and potential evapotranspiration. Daily data from the abovementioned meteorological stations (17123 and 17702) were used. As the stations are located outside of the boundaries of the watershed on both sides, the average of the records were used to represent the meteorological conditions over the watershed and take care of missing data occurring in any of the stations.

Figure 2 shows monthly average temperature and total precipitation data from October 1975 to September 2009. The smaller simulation period is displayed in solid lines. The linear trend lines within the simulation period show that there are no significant downward or upward trends for temperature and precipitation.

The cloudiness, solar radiation, and wind velocity data required by HSPF were also obtained from the respective stations. Dewpoint temperature was calculated from relative humidity records (Linsley et al. 1982). Potential evapotranspiration was taken to be the Penman Pan Evaporation and it was estimated using daily air temperature, dewpoint temperature, wind movement, and solar radiation (Te Chow et al. 1988).

Model parameters and calibration/validation

The large number of parameters required by HSPF is supplied to the model after their numerical values are determined by field observations, experiments, calibration, or literature surveys. The calibration of the model was carried out for the time period 1984–1995 (water years) and the validation between 1995 and 2004. Flow measurements at the Sarısu-İnönü station were utilized. The simulations were carried out with a 1-day interval. Calibration was carried out in a hierarchical manner where first yearly comparisons are conducted and the relevant parameters adjusted. As a next step, seasonal calibration was carried out.

Irrigation was applied to the segments PERLND 7 and PERLND 8. Based on a weighted average of irrigation water demands of crops grown in the region which are sugar beet and sunflower with limited amounts of orchards as obtained from land use maps, 200 mm of water was withdrawn from the stream (Köksal et al. 2011; Rinaldi 2001). This water was distributed throughout the irrigation season peaking in the middle of the season. Ninety percent of the water was applied to the soil surface. It was assumed that 5% would be lost by evaporation from interception storage and the remaining 5% was diverted to upper zone storage. Groundwater was set as the second alternative water withdrawal source for the case the stream went dry.

The most relevant parameters for the implementation of the HSPF and their values after calibration are displayed in Tables 2, 3, and 4 (Crawford 1999; Donigian and Davis 1978; Linsley 1992; USEPA 2000). Yearly flows after calibration and validation are shown in Fig. 3. There are missing years in the streamflow records, caused by short- (duration of a few days) or long- (duration of months or years) equipment failure or other causes. The agreement between yearly observations and simulations is 16%. Duda et al. (2012) provide a table where, for hydrological simulations, an agreement between 10 and 15% is considered good and between 15 and 25% fair.

Table 1 Sarısu watershed segments

Land segments	Characteristics	Average elevation (m)	Contributing area to R1 (km^2)	Contributing area to R2 (km^2)
PERLND 1	Pervious areas within cities	865	2.8	4.7
IMPLND 1	Impervious areas within cities	865	2.8	4.7
PERLND 2	Non-irrigated farmland	906	100.4	85.5
PERLND 3	Pasture	1033	111.0	93.9
PERLND 4	Barren land	1090	7.3	7.5
PERLND 5	Forest	965	8.5	1.0
PERLND 6	Wetland	1059	0.4	-
PERLND 7	Irrigated farmland	906	11.5	-
PERLND 8	Irrigated farmland	906	-	9.8
Stream segments	Total length (km)	Slope (m/km)		
R1	31.6	7		
R2	22.7	0.9		

Fig. 2 Monthly average temperature and total precipitation (October 1975–September 2009) in the Sarısu watershed
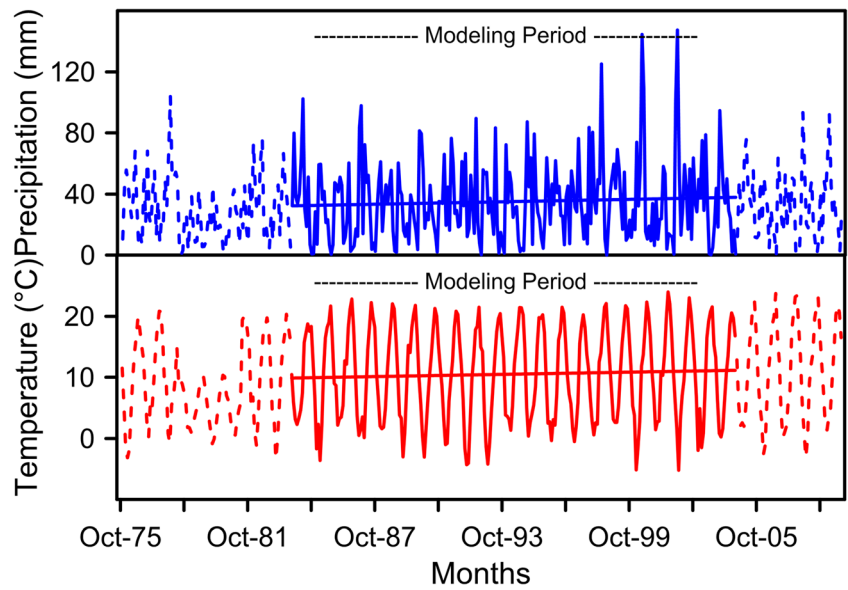
Based on this, the agreement can be put forward as being fair but very close to the "good" range. For monthly flows, the agreements between observations and simulations are lower, for some months considered to be even poor. The reasons lying behind poor monthly agreements are listed below.

a) Outside of the irrigation period, the water released from the reservoir consists of underflow. This underflow is not monitored properly and can be considered to be a major source of uncertainty in the streamflow records. The resulting uncertainty was not corrected and, as it will be mentioned later, carried forward into the future while the records were extended into the future. However, after climate simulations were carried out, two periods were compared with each other and as the underlying uncertainties are of the same nature, their effects canceled each other out.

b) The streamflow records show sharp increases in magnitude of short duration during the irrigation period and also during winter months. Some of these changes are not correlated with precipitation events at either meteorological stations (17123 and 17702) and consequently with the combined meteorological record. These discrepancies can be attributed to equipment malfunctioning. The same cancelation of underlying uncertainty as mentioned in the preceding paragraph also applied here.

c) Irrigation is not carried out with a regular schedule and the amounts withdrawn from the stream for irrigation are not known. The amount withdrawn is estimated based on the water need of the dominant irrigated crop in the region whose areal coverage and thus the water withdrawn however shows changes within years. These changes could not be simulated in the model.

Table 2 Parameters that do not change seasonally and are common to all watershed segments

Parameter	Description	Unit	Value	Comments
LZSN	Lower zone nominal storage	mm	200	Calibration
DEEPFR	Inflow to inactive groundwater	None	0	No water loss is assumed
AGWRC	Basic groundwater recession rate	1/day	0.98	Stream recession curves
BASETP	Fraction of potential E-T to be satisfied from baseflow	None	0	Riparian vegetation influence assumed to be negligible
AGWETP	Fraction of potential E-T to be satisfied from active groundwater	None	0.1	Calibration (exc. PERLND 6 which is 0.)
SNOWCF	Snow catch efficiency	None	1.3	Mean of physically realistic value range
COVIND	Maximum snowpack coverage	mm	38	Mean value of typical range
KMELT	Constant degree-day factor	mm/day. C	3.3	Calibration
RDCSN	Density of cold, new snow relative to water	None	0.2	Mean value of possible range
MWATER	Maximum water content of the snow pack	None	0.03	Common value from literature
MGMELT	Maximum rate of snowmelt by ground heat	mm/day	0.25	HSPF default value

Table 3 Parameters differing among watershed segments and not changing seasonally

	INFILT	NSUR	SHADE
Unit	mm/h		
Description	Index to the infiltration capacity of the soil	Manning's n	Fraction shaded from solar radiation
PERLND 1	2.5	0.05	0.33
IMPLND 1	-	0.05	0.33
PERLND 2	0.25	0.2	0.05
PERLND 3	0.25	0.25	0.1
PERLND 4	0.25	0.2	0
PERLND 5	0.25	0.2	0.2
PERLND 6	0.25	0.2	0
PERLND 7, 8	0.25	0.2	0.05
Comments	Based on soil hydrologic groups	Based on values from literature survey	Based on field observations

Projections into the future

The calibrated and validated HSPF model was used to make projections into the future using climatic projections. These projections were obtained by downscaling global climate model outputs. The projections as downscaled meteorological time series were fed into the HSPF model and the model run between the water years 1984 and 2099. For each meteorological time series required by HSPF, an ensemble of 400 members was used, thus requiring the application of the HSPF model 400 times. This multiple application of the model created an ensemble of streamflow time series whose statistical properties were subsequently examined.

Table 4 Parameters differing among watershed segments and changing seasonally

PERLND	January	February	March	April	May	June	July	August	September	October	November	December
Interception capacity, CEPS (mm)												
1	1.27	1.27	1.27	1.27	2.54	2.54	2.54	2.54	2.54	1.27	1.27	1.27
2	0.25	0.25	0.25	0.25	2.54	2.54	5.08	5.08	2.54	0.00	0.00	0.00
3	0.25	0.25	0.25	1.27	1.27	1.27	1.27	1.27	1.27	1.27	0.25	0.25
4	0.00	0.00	0.00	0.00	0.00	0.00	0.00	0.00	0.00	0.00	0.00	0.00
5	0.25	0.25	0.25	1.27	1.27	1.27	1.27	1.27	1.27	1.27	0.25	0.25
6	0.25	0.25	0.25	0.25	0.25	0.25	0.25	0.25	0.25	0.25	0.00	0.25
7, 8	0.25	0.25	0.25	0.25	2.54	2.54	5.08	5.08	2.54	0.00	0.00	0.00
Upper layer nominal storage, UZSN (mm)												
1, 5	2.54	2.54	2.54	2.54	2.54	2.54	2.54	2.54	2.54	2.54	2.54	2.54
2, 3, 7, 8	2.54	2.54	2.54	2.03	2.03	2.03	2.03	2.03	2.54	2.54	2.54	2.54
4	2.03	2.03	2.03	2.03	2.03	2.03	2.03	2.03	2.03	2.03	2.03	2.03
Interflow recession coefficient, IRC (1/day)												
1–8	0.3	0.3	0.3	0.7	0.7	0.3	0.3	0.3	0.3	0.3	0.3	0.3
Interflow parameter, INTFW												
1–8	1	1	1	1	3	3	3	3	3	3	3	1
Index to lower zone evapotranspiration, LZSN												
1	0.05	0.05	0.05	0.05	0.05	0.05	0.05	0.05	0.05	0.05	0.05	0.05
2	0.1	0.1	0.1	0.2	0.3	0.4	0.4	0.4	0.3	0.1	0.05	0.05
3	0.2	0.2	0.2	0.3	0.3	0.3	0.3	0.3	0.2	0.1	0.1	0.1
4	0.1	0.1	0.1	0.1	0.1	0.1	0.1	0.1	0.1	0.1	0.1	0.1
5	0.1	0.1	0.1	0.2	0.2	0.2	0.2	0.2	0.2	0.1	0.05	0.05
6	0.6	0.6	0.6	0.6	0.6	0.6	0.6	0.6	0.6	0.6	0.6	0.6
7, 8	0.2	0.2	0.2	0.3	0.4	0.4	0.4	0.4	0.1	0.05	0.01	0.01

The downscaled meteorological time series

The meteorological time series belonging to the stations 17123 and 17702 and required by HSPF were downscaled from two general circulation models (GCMs), namely the Canadian Climate Center (CGCM3.1(T63)) and the Met Office Hadley Centre (2012) (HadCM3) models with three Special Report on Emission Scenarios, A1B, A2, and B2 (IPCC 2007). SDSM (Statistical DownScaling Model) (Wilby and Dawson 2007; Wilby et al. 2002) was utilized together with an automated regression-based statistical downscaling tool (ASD, Automated Statistical Downscaling) for automatic predictor selection based on backward stepwise regression and partial correlation coefficients (Hessami et al. 2008). The complete downscaling procedure is described in detail in (Göncü and Albek 2015). Four GCM–scenario combinations to encompass a wide range of possible future climatic conditions were considered as given in Table 5.

Figure 4 displays how the yearly average temperature and yearly total precipitation ensembles evolve between the water years 1984 and 2099. The lower and upper limits of the ranges are 25th and 75th percentiles of 400 time series as produced with the scenario generator of SDSM, smoothed using 10-year medians for better visual clarity. The box and whisker plots at the ends of the ranges represent the first and last 30 years of the 116-year periods and visualize how the temperature and precipitation changed within this period. The box and whisker plots in Fig. 5 show 30-year period median differences for the whole ensemble and its breakdown into the GCM–scenario combinations. Disregarding the data below and above 25th and 75th percentiles, respectively, the 400 time series encompass a temperature increase between 2.8 and 4.5 °C and a precipitation change between − 108 and − 35 mm within the 86-year periods between the centers of the 30-year periods. For the individual GCM–scenario combinations, the highest temperature increase is seen in the H3_A2 combination and the lowest increase in the C3_A1B combination. For
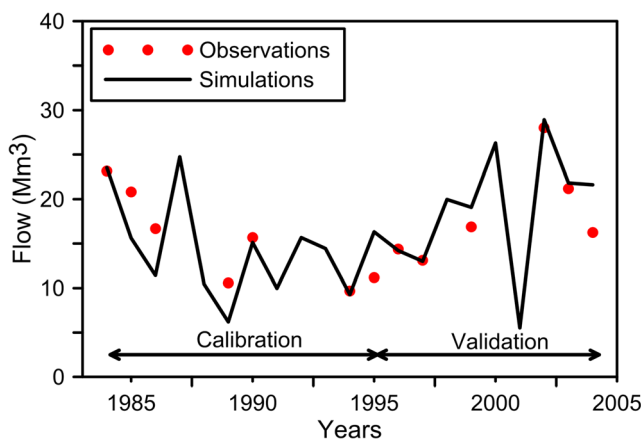

Fig. 3 Observed and simulated yearly streamflows at the Sarısu-İnönü station

precipitation, C3_A2 shows the largest decrease while H3_B2 records the smallest reduction.

The period differences were calculated using a Hodges–Lehmann type of estimator (Eq. (1))

$$D = \left(P_{i,m} - P_{i,n}\right) \, i = 1..100, m = 2070..2099; n$$
$$= 1984..2013 \tag{1}$$

where i stands for ensemble members and m and n year indices from different time periods, respectively. P are the projections and D is their difference (Esterby 1996). For each period and each ensemble member, there are 30 values and thus 900 differences among the periods from which statistical properties are calculated subsequently and displayed as boxplots.

The differences above indicate a substantial change in temperatures and precipitation. For temperature, the median increase is 2.9 °C which considering an overall median of 12.2 °C calculated from 46,400 values (400 yearly temperatures × 116 years) gives rise to a 24% increase. For precipitation, the median decrease is 72 mm which over an overall median of 365 mm amounts to a decrease of 20%. For the other meteorological time series required by HSPF, the changes are modest. Cloudiness decreases by 6.5%, relative humidity by 0.5%, and wind velocity increases by 4%.

Figures 6 and 7 present how monthly average temperatures and total precipitation change over the 86-year periods, respectively. The figures display the period differences for 400 ensemble members irrespective of the individual GCM–scenario combinations. The differences are calculated with Eq. (1) and median absolute deviations (MAD) (Eq. (2)) are displayed as error bars over the monthly median differences.

$$MAD = \mathrm{median}(|Di - \mathrm{median}(Di)|) \, for \, i = 1...400 \tag{2}$$

In Fig. 6, temperatures increase in all months and the highest increases are encountered in summer months. The upper part of the plot shows how the much the increase is over the overall monthly median. Here, the largest change occurs in January. Though the increase is small compared with other months, the change over the overall median is large as the overall temperature median is small in January. For precipitation (Fig. 7), the smooth pattern over the year as in Fig. 6 is not seen. In 3 months of the year, namely February, March, and September, relatively small increases are encountered. The largest decreases are in May and June. The changes over the overall median are displayed as numbers in the lower part of the plot. Here, May, June, and July show the largest decreases. The comparatively wide MAD ranges show the large deviations among the GCM–scenario combinations.

Table 5 GCM–scenario combinations

Combination	GCM	Scenario	Scenario Characteristics [2]
C3–A1B	Canadian Climate Center CGCM3.1	SRES–A1B	Market-oriented world with the fastest economic growth among the scenarios and strong regional interaction
C3–A2	Canadian Climate Center CGCM3.1	SRES–A2	More emphasis on economy than A1B in a strongly
H3–A2	Met Office Hadley Centre HadCM3	SRES–A2	heterogeneous world, less rapid development, and spread of new technologies for abatement of carbon dioxide buildup
H3–B2	Met Office Hadley Centre HadCM3	SRES–B2	Emphasis on local solutions with the development of new technologies at a rate between the foregoing scenarios

HSPF simulations with the projections

HSPF was run 400 times with the 400 projection sets (each set comprising of 7 time series required by HSPF). The simulation period, as mentioned above, was between 1984 and 2099 in terms of water years. The simulation interval was set as 1 day.

In the simulations, the only time-changing component was the time series. The parameters used by HSPF were considered as constant within the simulation period as well as the irrigation schedule and the watershed and

stream characteristics. This imposes a limitation on the projections as some parameters will likely change as climatic conditions shift. An example is the interception capacity of vegetation. Increased droughts or highly wet periods will influence foliage patterns and thus the amount of precipitation intercepted. Likewise, the hydrological response of the soil will also show changes as reflected in the infiltration capacity, etc. Such possible alterations were not considered. Besides climatic conditions, land use patterns also will be changing. However, there is no way to predict how the future use of the watershed will evolve. Therefore, it was assumed that the watershed will remain in its present state (in the state HSPF was calibrated and validated) while the climatic conditions change within the limits of the GCM–scenario combination predictions.
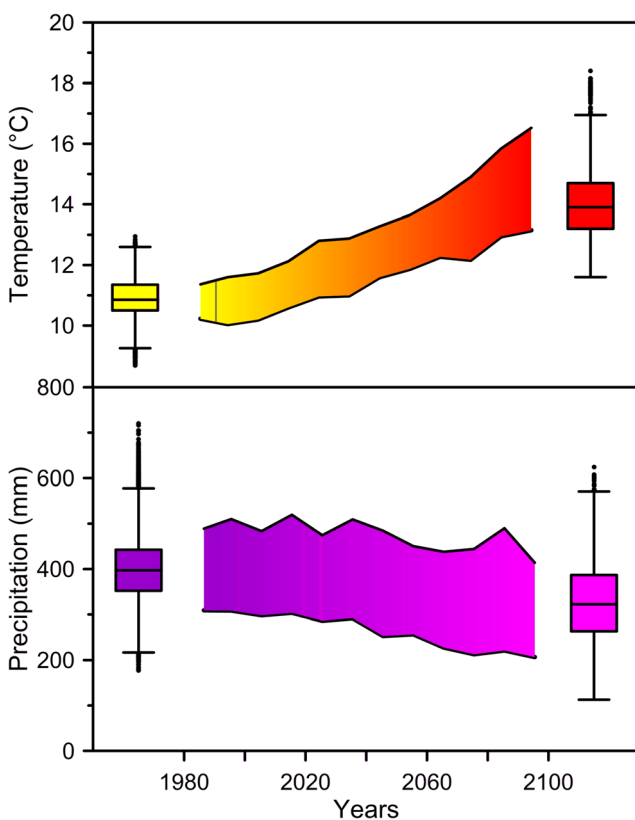

Fig. 4 Yearly average temperature (upper plot) and total precipitation (lower plot) ensembles (1984–2099). Lower and upper limits of the ranges are 25th and 75th percentiles of 400 time series smoothed using 10-year medians. The box and whisker plots represent the first and last 30 years of the 116-year periods. The whiskers are 1.5 × IQR (interquartile range)
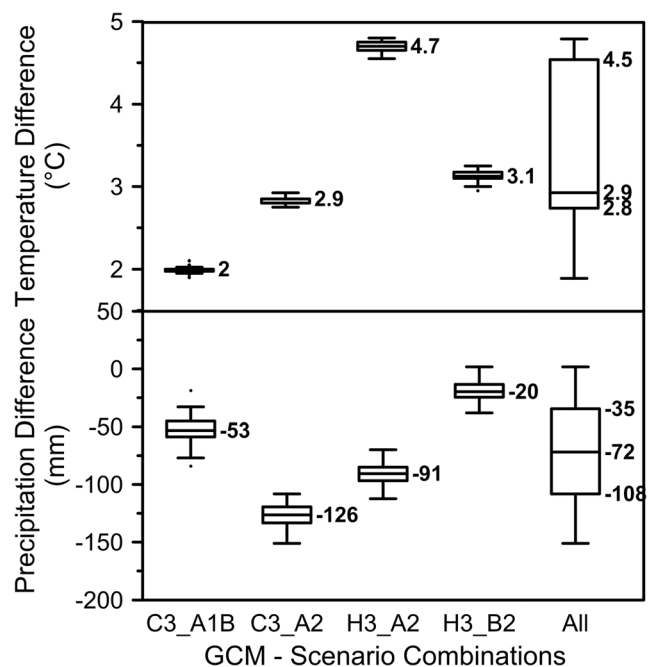

Fig. 5 Box and whisker plots of 30-year period median differences for the whole ensemble and breakdown into the GCM–scenario combinations. Upper plot is for yearly average temperature and lower plot for yearly total precipitation. The whiskers are 1.5 × IQR (interquartile range)
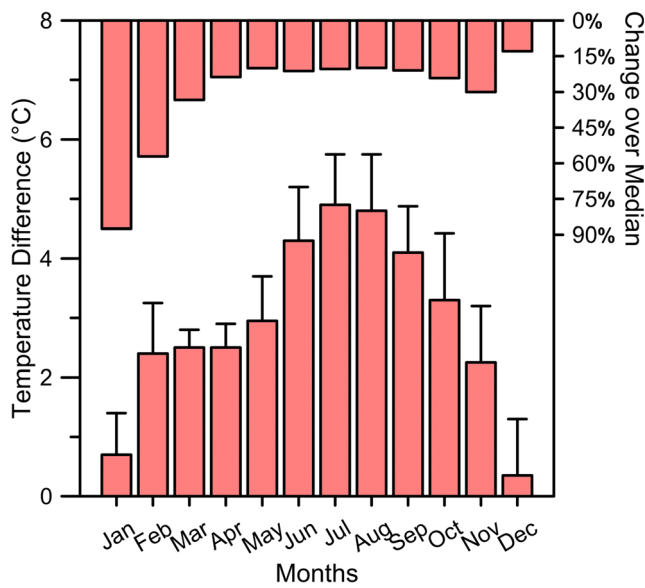
Fig. 6 Monthly average temperature period differences for 400 ensemble members. The error bars are median absolute deviations. The upper reversed bars represent the increase over the overall monthly median

Streamflow projections

Four hundred streamflow projections were obtained as a result of the simulations with HSPF with the projection sets as described before. The outflow of the Sarısu stream (stream reach R2) was chosen to investigate the change in streamflow with changing meteorological conditions. Figure 8 displays how the 400 ensemble members which comprise of all GCM–scenario combinations evolve and decrease between the water
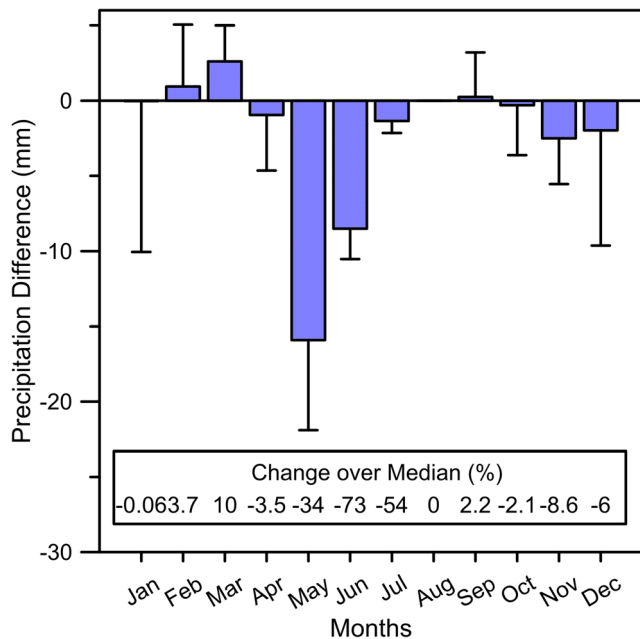
Fig. 7 Monthly total precipitation period differences for 400 ensemble members. The error bars are median absolute deviations. The numbers in the box represent the change over the overall monthly median

years 1984 and 2099. The lower and upper limits of the ranges are 25th and 75th percentiles of the streamflow time series obtained from HSPF, smoothed using 10-year medians for better visual clarity. The box and whisker plots at the ends of the ranges represent the first and last 30 years of the 116-year periods to help to visualize how the streamflow changed within this period. The medians in these first and last 30-year periods are 27.3 and 17.5 Mm^3, respectively which leads to a decrease of 9.8 Mm^3 over 86 years.

Figure 9 shows the 30-year period median differences for the whole ensemble and its breakdown into the GCM–scenario combinations. The period differences were calculated with the Hodges–Lehmann type of estimator in Eq. (1). Not taking into consideration the data outside the 25th and 75th percentiles, the 400 time series encompass a streamflow decrease between 4 and 12 Mm^3 within the 86-year periods between the centers of the 30-year periods. The median decrease is 9 Mm^3 and represents a change of − 40% over an overall median streamflow of 22.3 Mm^3. Comparing this reduction in streamflow with the 9.8 Mm^3 reduction obtained above by simply considering the difference between the two start and end period 30-year medians shows that the two approaches (simple median difference and Hodges–Lehmann-type difference estimator) give similar results. The corresponding decrease in precipitation was found to be 19% in the "The downscaled meteorological time series" section. The decrease of 40% in streamflow is almost twice this value and the effects of the increase in temperatures resulting in larger evapotranspiration volumes are evident.

The behavior of the streamflows across months is displayed in Fig. 10. The box and whisker plots for any month show statistics calculated from 46,400 values (116 years × 400 combinations). The first 3 months of the year display a number of outliers larger than 50 Mm^3 which mostly belong to 2
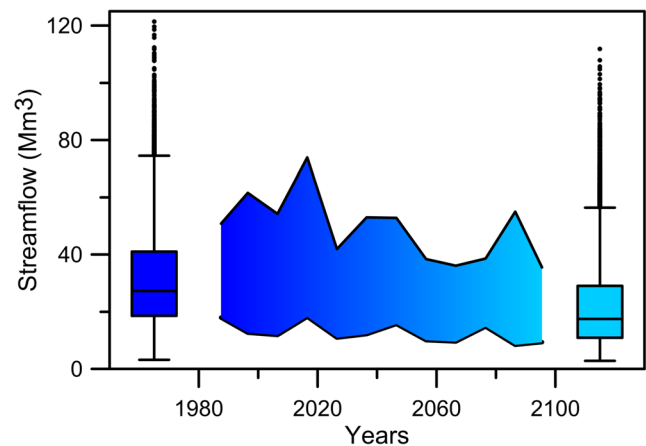

Fig. 8 Yearly total streamflow ensembles (1984–2099). Lower and upper limits of the ranges are 25th and 75th percentiles of 400 time series smoothed using 10-year medians. The box and whisker plots represent the first and last 30 years of the 116-year periods. The whiskers are 1.5 × IQR (interquartile range)
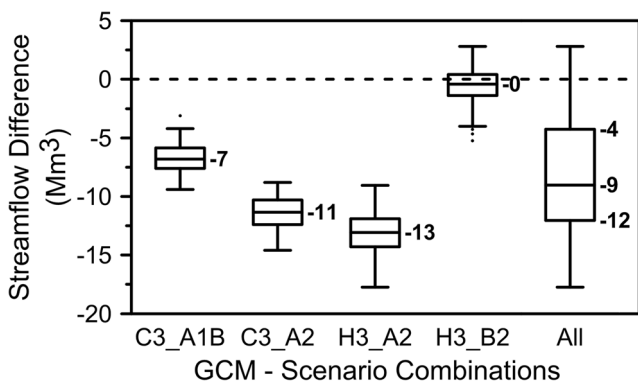
Fig. 9 Box and whisker plots of 30-year period median differences of yearly total streamflow for the whole ensemble and breakdown into the GCM–scenario combinations. The whiskers are 1.5 × IQR (interquartile range)

in the equalization processes in the watershed soils. The largest differences in streamflows are encountered in the first half of the year where the streamflows are already higher due to runoff. The decreases are modest in the irrigation period which is an expected result as these flows are mostly made up from reservoir releases and were designed in the simulations not to change over the simulation period.

The distributions of the streamflows in the two 30-years at the beginning and end of the 116-year simulation periods (Fig. 12) display clearly the change (decrease) in the medians. The second and comparatively drier period (upper plot in Fig. 12) is more skewed to the left, indicating the shifting of the majority of flows to lower values. The second period also displays a higher kurtosis with flatter tails (especially on the right as compared with the first period). The contrasting red lines are lognormal distributions which fit closely to the histograms. The lognormality of the data is not lost between the periods while the distribution parameters (skewness and kurtosis) do.

years (2036 in the C3_A1B and 2042 in the H3_A2 combinations) of extraordinarily high streamflows (200 values). These high flows present themselves as yearly outliers above around 80 Mm^3 in the boxplots in Fig. 8. The remaining outliers, for every month, do not exceed 15 Mm^3. Only in the months of August and September, very few outliers are encountered. In these months, the flows are also low, released more steadily from the reservoir and withdrawn from the stream for irrigation. The irrigation release from the reservoir can be erratic, depending on the demands and water levels in the reservoir, as shown in the outliers of the preceding months.

The 30-year median differences for the streamflows (Fig. 11) display decreases of varying magnitude all over the months. The two precipitation increases in February and March (Fig. 7) do not show up in the streamflows and are lost
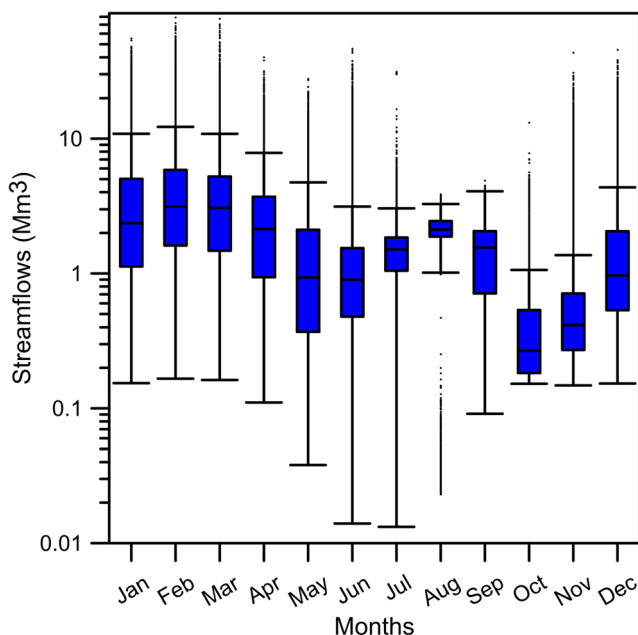
Temperature–precipitation–streamflow correlations

Correlations were established for yearly total streamflow with the two principal drivers of watershed processes: yearly average temperature and yearly total precipitation. Four hundred corresponding correlation coefficients each were calculated for temperature vs. precipitation, temperature vs. streamflow, precipitation vs. streamflow, temperature-adjusted precipitation vs. streamflow, and temperature-adjusted precipitation vs. temperature-adjusted streamflow.
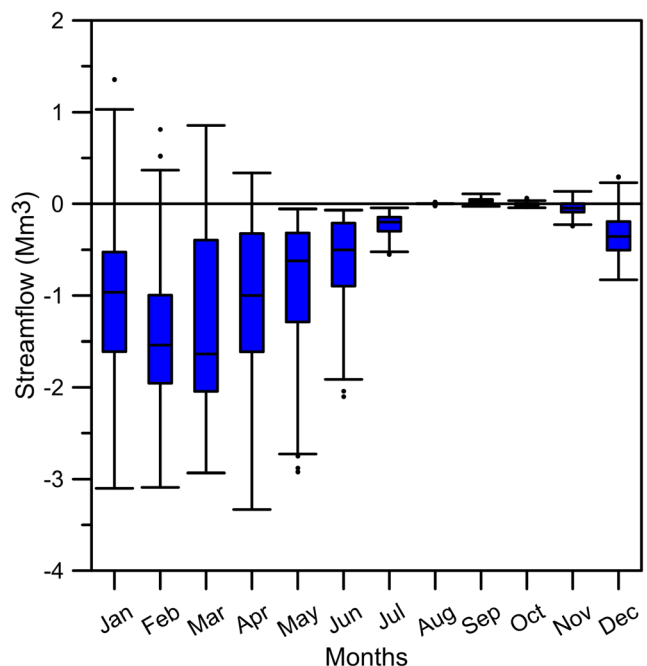

Fig. 10 Box and whisker plots for monthly total streamflow over the simulation period (1984–2099). The whiskers are 1.5 × IQR (interquartile range)

Fig. 11 Box and whisker plots of 30-year period median differences of monthly total streamflow for the whole ensemble. The whiskers are 1.5 × IQR (interquartile range)
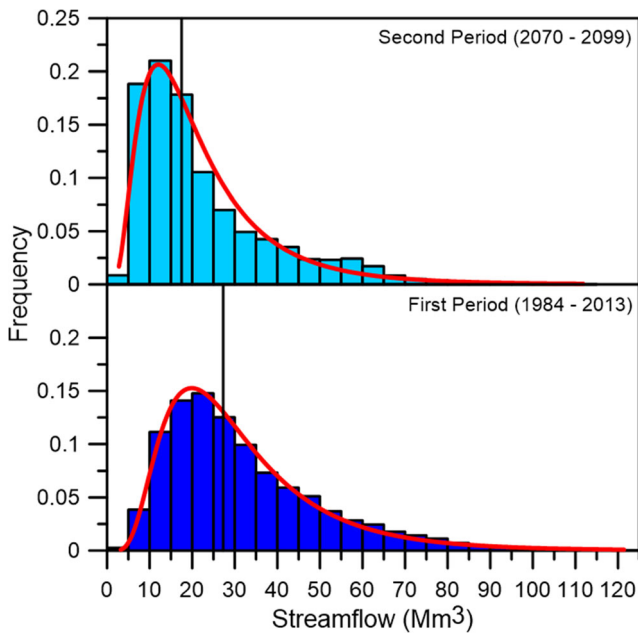
Fig. 12 Histograms of yearly total streamflows in the first (1984–2013, lower plot) and second (2070–2099, upper plot) periods. The vertical lines are the period medians. The red lines represent the lognormal fit

A nonparametric correlation coefficient, Kendall's Tau, was selected to establish the correlations. Kendall's Tau (Helsel and Hirsch 1993) is a rank-based measure of the strength of the monotonic relationship between two data sets, being well suited for skewed relationships.

The test statistic is Kendall's S which is calculated (after ordering all data pairs by increasing x, the independent variable) by subtracting the number of "discordant pairs" M which are those (x-independent variable, y-dependent variable) pairs for which y decreases with increasing x, from the number of "concordant pairs" P which are the (x, y) pairs for which y increases as x increases. In other words:

$$S = P - M \qquad (3)$$

where P is the times when $y_i < y_j$ for all $i < j$, and M is the times when $y_i > y_j$ for $i < j$ for all $i = 1,2,..(n-1)$ and $j = 2,3,..n$, where n is the number of data pairs (Helsel and Frans 2006).

Kendall's Tau correlation coefficient is then defined as

$$\tau = \frac{s}{n(n-1)/2} \qquad (4)$$

τ changes between -1 and $+1$ like its parametric counterpart, Pearson's r.

Temperature adjustment for precipitation and streamflow are done, to further gain insight into the relationships among the two watershed process drivers (temperature and precipitation) and the watershed output (streamflow). While a two-way relationship between temperature and precipitation can be

conceived, a one-way relationship exists clearly between temperature and streamflow, and precipitation and streamflow. Streamflow is inversely related to temperature and positively related to precipitation, as expected. Temperature adjustment of precipitation and streamflow removes the mutual dependence between them and the relationship of streamflow to precipitation without the intervention of temperature can be studied. The idea and procedure are analogous to the concept of partial correlations (Wetcher-Hendricks 2014).

Temperature adjustment of precipitation was carried out by first establishing a functional relationship between the temperature and precipitation. Nonparametric regression was applied due to the non-normality of the distributions of the respective data sets (Helsel 1987). The slope of the regression line (Theil slope) is calculated by comparing each data pair to all others in a pairwise fashion which results in $n(n-1)/2$ slopes as:

$$\text{Slope}_k = \frac{y_j - y_i}{x_j - x_i} \text{ for all } i < j; i = 1, 2, \ldots(n-1), j$$

$$= 2, 3, \ldots, n, k = 1, 2, \ldots \frac{n(n-1)}{2} \qquad (5)$$

The median of all the slopes (for 116 data pairs, there are 6670 slopes) gives the Theil slope. The intercept is then calculated as:

$$\text{Intercept} = \text{median}(y) - \text{slope} \times \text{median}(x) \qquad (6)$$

This method of finding the intercept ensures that the nonparametric regression line (Kendall–Theil line) goes through the median of the data set (Helsel and Hirsch 1993). Thus, 400 regression lines with 400 intercepts and slopes are prepared for all the GCM–scenario combinations. The temperature-adjusted precipitation (TAP) is found by subtracting the corresponding precipitation obtained from the regression equation with temperature from the observed precipitation as

$$\text{TAP}_m(t) = P_m(t) - \text{intercept}_m - \text{slope}_m T_m(t) \text{ for all } m$$

$$= 1, 2, \ldots 400; t = 1, 2, \ldots 116 \qquad (7)$$

where the subscript m stands for the individual GCM–scenario combinations and t stands for the years. Temperature adjustment for streamflow is carried out in the same pattern and temperature-adjusted streamflows (TAS) are found.

An example of the temperature adjustment process is shown for a particular GCM–scenario combination (the first time series form the GCM–C3_A1B scenario combination) in Fig. 13.

The relationship between precipitation (P) and streamflow (S) is a positive one with a median Kendall Tau value of 0.54. The Tau values range from a minimum of 0.43 to a maximum

of 0.65 and all 400 correlations between P and S from all GCM–scenario combinations are significant at 95% confidence level. Streamflow is negatively correlated with temperature (T) with a median Kendall Tau value of − 0.30. The Tau values range from a minimum of − 0.027 to a maximum of − 0.50. Here, for negative correlation, the range is from 0 to − 1, with values close to zero considered to represent a poor correlation and vice versa. Therefore, − 0.027 is considered a minimum and − 0.50 a maximum while from a pure mathematical viewpoint the case is reversed. Among the 400 Tau values, 91 (22.8%) are not significant at 95% confidence level. These values lie close to the minimum of − 0.027 and belong exclusively to the GCM–H3_B2 scenario combination. Temperature and precipitation are also negatively correlated with a median Kendall Tau value of − 0.34. The Tau values range from a minimum of − 0.052 to a maximum of − 0.55. Thirty-eight (9.5%) Tau values are not significant at 95% confidence level. Again, these lie close to the minimum of − 0.052 and belong to the GCM–H3_B2 scenario combination.

The correlation between temperature-adjusted precipitation (TAP) and temperature-adjusted streamflow (TAS) results in a median Kendall Tau value of 0.48 with no insignificant
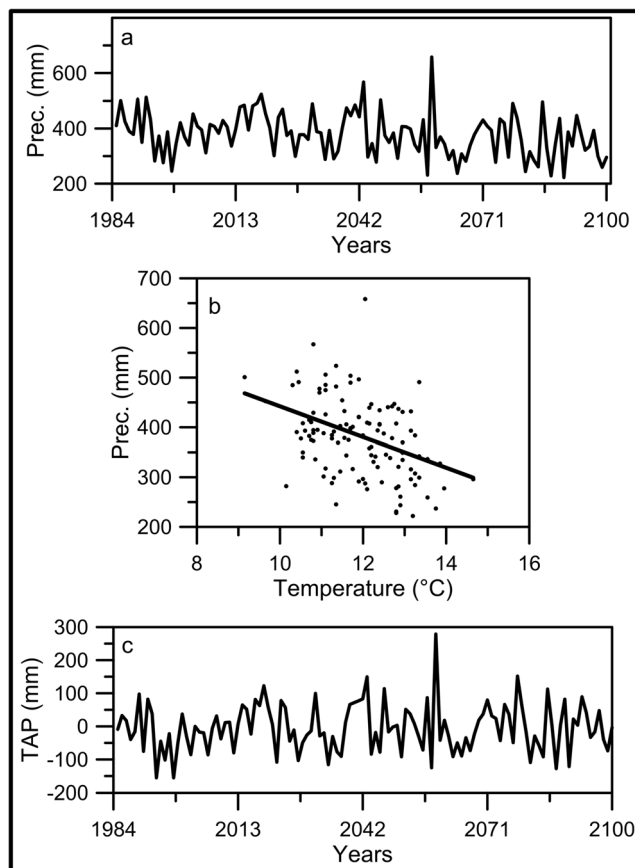

Fig. 13 Temperature adjustment process of precipitation for the first ensemble member. Plot a: unadjusted precipitation; plot b: Kendall–Theil line between temperature and precipitation; plot c: temperature-adjusted precipitation

correlations and minimum and maximum limits of 0.28 and 0.62, respectively. Thus, temperature adjustment decreased the correlation (from 0.54 to 0.48). Temperature is inversely related to both precipitation and streamflow, and the removal of this double-effect correlation affected the relationship between precipitation and streamflow, though not on a large scale (12% reduction in the median quantities).

The correlations for the two 30-year periods separately at the beginning and end of the whole 116-year simulation periods deviate significantly from the whole period correlations. First of all, the correlations T vs. P and T vs. S are predominantly insignificant (71% and 56%, respectively in the first period and 79% and 83%, respectively in the second period out of 400 combinations). Thus, it is not practical to form regressions between uncorrelated quantities. However, S is predominantly significantly correlated to P. In the first period, the median Kendall Tau is 0.46 and the values range from a minimum of 0.15 to a maximum of 0.71 (8 insignificant correlations, 2%). In the second period, these values become 0.55, − 0.028, and 0.72 (54 insignificant correlations, 14%). It can be seen that the streamflows became more strongly related to precipitation later in the simulation period, despite the higher number of insignificant correlations. It is also noteworthy here that the insignificant correlations are found among all scenarios and not confined to solely the GCM–H3_B2 scenario combination as observed before for the whole period.

Conclusions and recommendations

Streamflow projections into the future were obtained with the use of HSPF with meteorological input from downscaling of GCM–scenario combinations. The 400 meteorological input sets enabled to obtain an equivalent streamflow projection set comprising 400 time series. As pointed out in the "Introduction" section, acquiring a cloud of streamflow projections gives the user and analyzer of this type of future information the distinctive advantage of possessing a range of values which can still be reduced to easier manageable quantities like the median (a measure of central tendency), the interquartile range (a measure of spread), and minimums and maximums (the outer limits of the range). Thus, the user who is provided with the task of planning for a future with a different climate is confronted, in a positive sense, with likely outcomes in the future to which to adapt, has more information to use in plans and develop alternatives.

The temperature and precipitation ensembles show a grim future with respect to climatic conditions in the watershed in question which will certainly be replicated in numerous other watersheds around the world as the GCM projections display. A median increase of 2.9 °C in temperature and 72 mm precipitation decrease covering a likely range of scenario

outcomes are values which will certainly endanger the already sensitive hydrological and ecological balance. The resulting change in streamflows, mostly in the negative direction, will be strongly felt by the stakeholders in the watershed. 2.9 °C is the median increase and as evidenced in Fig. 5, higher temperature increases (with a maximum of 4.5 °C) seem also possible at the end of the twenty-first century. The pessimistic scenarios also pointed towards larger precipitation decreases than 72 mm (105 mm). Higher temperatures coupled with lower precipitations are likely to produce synergistic outcomes which can lead from public health-endangering heat waves to prolonged drought events, among others like devastating forest fires or invasive species, which will have environmental and public effects as well as economic consequences.

The water resources of the Sarısu watershed are important for domestic, industrial, and agricultural users. Though it can be anticipated that all users will feel an ever-increasing demand for water, there are projects underway which develop actions to decrease water consumption. With the usual application of spray irrigation, much irrigation water is lost due to evaporation. The transition to other water-saving practices of irrigation (subsurface, drip, etc.) will be a great leap towards the adaptation to a warmer and drier climate with decreased streamflows. Likewise, reductions in water wastefulness in households and industry will help in the adaptation process.

References

Abdulla F, Eshtawi T, Assaf H (2009) Assessment of the impact of potential climate change on the water balance of a semi-arid watershed. Water Resour Manag 23:2051–2068

Al-Abed N, Al-Sharif M (2008) Hydrological modeling of Zarqa River Basin - Jordan using the Hydrological Simulation Program-FORTRAN (HSPF) model. Water Resour Manag 22:1203–1220

Albek E (2003) Estimation of point and diffuse contaminant loads to streams by non-parametric regression analysis of monitoring data. Water Air Soil Pollut 147:229-243 doi:https://doi.org/10.1023/a:1024592815576

Albek M, Albek E (2003) Use of HSPF in estimating future influences of climate change on watersheds. WIT Trans Ecol Environ 60:55–65. https://doi.org/10.2495/RM030061

Albek M, Ogutveren UB, Albek E (2004) Hydrological modeling of Seydi Suyu watershed (Turkey) with HSPF. J Hydrol 285:260–271

Baloch MA, Ames DP, Tanik A (2015) Hydrologic impacts of climate and land-use change on Namnam Stream in Koycegiz Watershed, Turkey. Int J Environ Sci Te 12:1481–1494

Bicknell BR, Imhoff JC, Kittle JL Jr, Jobes TH, Donigian AS Jr (2001) Hydrological Simulation Program - Fortran (HSPF). User's Manual for Release 12. In: U.S. EPA National Exposure Research Laboratory, Athens, GA, in cooperation with U.S. Geological Survey, Water Resources Division, Reston, VA

Canadian Centre for Climate Modelling and Analysis (2012) University of Victoria. http://www.cccma.ec.gc.ca/data/cgcm3/cgcm3.shtml. Accessed 2008

Choi W, Deal BM (2008) Assessing hydrological impact of potential land use change through hydrological and land use change modeling for the Kishwaukee River basin (USA). J Environ Manage 88:1119–1130

Chung ES, Park K, Lee KS (2011) The relative impacts of climate change and urbanization on the hydrological response of a Korean urban watershed. Hydrol Process 25:544–560

Climate Impacts LINK Project (2012) NCAS British Atmospheric Data Centre. http://badc.nerc.ac.uk/view/badc.nerc.ac.uk__ATOM__dataent_linkdata. Accessed 2008

Crawford NH (1999) Hydrologic Journal - Snowmelt Calibration. Hydrocomp, Inc. www.hydrocomp.com. 2010

Donigian ASJ, Davis HHJ (1978) User's Manual for Agricultural Runoff Management (ARM) Model. In., vol EPA- 600/3-78-080.

Duda PB, Hummel PR, Donigian ASJ, Imhoff JC (2012) BASINS/HSPF:Model Use, Calibration and Validation. Transactions of the ASABE 55:1523-1547 doi:10.13031/2013.42261

ECMWF ERA-40 data (2012) ECMWF Data Server. http://www.ecmwf.int/research/era/do/get/era-40. Accessed 2008

Esterby SR (1996) Review of methods for the detection and estimation of trends with emphasis on water quality applications. Hydrol Process 10:127–149

Goncu S, Albek E (2007) Modeling the effects of climate change on different land uses. Water Sci Technol 56:131-138 doi. https://doi.org/10.2166/Wst.2007.444

Goncu S, Albek E (2008) Modeling climate change impacts on suspended and dissolved water quality constituents in watersheds. Fresenius Environ Bull 17:1501–1510

Goncu S, Albek E (2010) Modeling climate change effects on streams and reservoirs with HSPF. Water Resour Manag 24:707–726. https://doi.org/10.1007/s11269-009-9466-6

Göncü S, Albek E (2015) Statistical downscaling of meteorological time series and climatic projections in a watershed in Turkey. Theoretical Appl Climatol:1–21. https://doi.org/10.1007/s00704-015-1563-2

He MX, Hogue TS (2012) Integrating hydrologic modeling and land use projections for evaluation of hydrologic response and regional water supply impacts in semi-arid environments. Environ Earth Sci 65:1671–1685

He ZL, Wang Z, Suen CJ, Ma XY (2013) Hydrologic sensitivity of the Upper San Joaquin River Watershed in California to climate change scenarios. Hydrol Res 44:723–736

Helsel DR (1987) Advantages of nonparametric procedures for analysis of water-quality data. Hydrol Sci J 32:179-190 doi:https://doi.org/10.1080/02626668709491176

Helsel DR, Frans LM (2006) Regional Kendall test for trend. Environ Sci Technol 40:4066–4073. https://doi.org/10.1021/es051650b

Helsel DR, Hirsch RM (1993) Statistical methods in water resources. Elsevier Science

Hessami M, Gachon P, Ouarda TBMJ, St-Hilaire A (2008) Automated regression-based statistical downscaling tool. Environ Model Softw 23:813–834. https://doi.org/10.1016/j.envsoft.2007.10.004

IPCC (2007) Climate Change 2007: The Physical Science Basis. Contribution of Working Group I to the Fourth Assessment Report of the Intergovernmental Panel on Climate Change. In: Solomon S et al (eds) Cambridge University Press. United Kingdom and New York, NY, USA, Cambridge, p 996

Jun KS, Chung ES, Sung JY, Lee KS (2011) Development of spatial water resources vulnerability index considering climate change impacts. Sci Total Environ 409:5228–5242

Kalnay E et al (1996) The NCEP/NCAR 40-year reanalysis project B. Am Meteorol Soc 77:437–471. https://doi.org/10.1175/1520-0477(1996)077<0437:Tnyrp>2.0.Co;2

Kim Y, Chung ES (2014) An index-based robust decision making framework for watershed management in a changing climate. Sci Total Environ 473:88–102

Kistler R et al (2001) The NCEP-NCAR 50-year reanalysis: monthly means CD-ROM and documentation. B Am Meteorol Soc 82: 247–267. https://doi.org/10.1175/1520-0477(2001)082<0247:Tnnyrm>2.3.Co;2

Köksal ES, Güngör Y, Yildirim YE (2011) Spectral reflectance characteristics of sugar beet under different levels of irrigation water and relationships between growth parameters and spectral indexes. Irrig Drain 60:187–195. https://doi.org/10.1002/ird.558

Linsley RK (1992) Water Resources Engineering. McGraw-Hill

Linsley RK, Kohler MA, Paulhus JLH (1982) Hydrology for Engineers. McGraw-Hill, New York

Lopez SR, Hogue TS, Stein ED (2013) A framework for evaluating regional hydrologic sensitivity to climate change using archetypal watershed modeling. Hydrol Earth Syst Sc 17:3077–3094

Lumb AM, McCammon RB, Kittle JL Jr (1994) Users manual for an expert system (HSPexp) for calibration of the Hydrologic Simulation Program–Fortran. In: vol 94-4168. U.S. Geological Survey Water-Resources Investigations Report, p 102

Mitsova D (2014) Coupling Land Use Change Modeling with Climate Projections to Estimate Seasonal Variability in Runoff from an Urbanizing Catchment Near Cincinnati. Ohio Isprs Int Geo-Inf 3: 1256–1277

Monitoring Stations Management System (2010) General Directorate of State Hydraulic Works. http://rasatlar.dsi.gov.tr/. Accessed 2010

Mukundan R et al (2013) Suspended sediment source areas and future climate impact on soil erosion and sediment yield in a New York City water supply watershed, USA. Geomorphology 183:110–119. https://doi.org/10.1016/j.geomorph.2012.06.021

Ng HYF, Marsalek J (1992) Sensitivity of streamflow simulation to changes in climatic inputs. Hydrol Res 23:257–272

NRC (2010) Advancing the Science of Climate Change. The National Academies Press

Ranatunga T, Tong STY, Sun Y, Yang YJ (2014) A total water management analysis of the Las Vegas Wash watershed. Nevada Phys Geogr 35:220–244

Rinaldi M (2001) Application of EPIC model for irrigation scheduling of sunflower in Southern Italy. Agric Water Manag 49:185–196

Rosenberg EA, Keys PW, Booth DB, Hartley D, Burkey J, Steinemann AC, Lettenmaier DP (2010) Precipitation extremes and the impacts of climate change on stormwater infrastructure in Washington State. Climatic Change 102:319–349

Taner MU, Carleton JN, Wellman M (2011) Integrated model projections of climate change impacts on a North American lake. Ecol Model 222:3380–3393

Te Chow V, Maidment DR, Mays LW (1988) Applied Hydrology. McGraw-Hill, New York

TUMAS Meteorological Data Archive and Management System. (2010) Turkish State Meteorological Service. http://tumas.mgm.gov.tr/wps/portal/. Accessed 2010

USEPA (2000) BASINS technical note 6 estimating hydrology and hydraulic parameters for HSPF. In., vol EPA-823-R00-012. US EPA Office of Water, United States, p 34

USEPA (2015) BASINS 4.1 (Better Assessment Science Integrating point & Non-point Sources) Modeling Framework. National Exposure Research Laboratory, RTP, North Carolina

Wetcher-Hendricks D (2014) Analyzing quantitative data: an introduction for social researchers (1). Wiley, Somerset, US

Wilby RL, Dawson CW (2007) Statistical Downscaling Model SDSM User Manual, Version 4.2. In. Loughborough University,

Wilby RL, Dawson CW, Barrow EM (2002) SDSM - a decision support tool for the assessment of regional climate change impacts. Environ Model Softw 17:147–159

Yan CA, Zhang WC, Zhang ZJ (2014) Hydrological modeling of the Jiaoyi watershed (China) using HSPF model. Sci World J

Yang JS, Chung ES, Kim SU, Kim TW (2012) Prioritization of water management under climate change and urbanization using multi-criteria decision making methods. Hydrol Earth Syst Sc 16:801–814